Quaternary Science Advances 10 (2023) 100079

Contents lists available at ScienceDirect

Quaternary Science Advances

journal homepage: www.sciencedirect.com/journal/quaternary-science-advances

Review

Cryptotephras in the marine sediment record of the Edisto Inlet, Ross Sea: Implications for the volcanology and tephrochronology of northern Victoria Land, Antarctica

Alessio Di Roberto [a,*], Giuseppe Re [a], Bianca Scateni [a], Maurizio Petrelli [b], Tommaso Tesi [c], Lucilla Capotondi [d], Caterina Morigi [e], Giacomo Galli [e,f], Ester Colizza [g], Romana Melis [g], Fiorenza Torricella [g,h], Patrizia Giordano [c], Federico Giglio [c], Andrea Gallerani [d], Karen Gariboldi [e]

[a] Istituto Nazionale di Geofisica e Vulcanologia, Sezione di Pisa, via C. Battisti 53, 56125, Pisa, Italy
[b] Dipartimento di Fisica e Geologia, Università degli Studi di Perugia, Via Alessandro Pascoli, 06123, Perugia, Italy
[c] CNR - Istituto di Scienze Polari, Area della Ricerca di Bologna, Via P. Gobetti 101, 40129, Bologna, Italy
[d] CNR - Istituto di Scienze Marine, Area della Ricerca di Bologna, Via P. Gobetti 101, 40129, Bologna, Italy
[e] Dipartimento di Scienze della Terra, Università di Pisa, Via S. Maria 53, 56126, Pisa, Italy
[f] Campus Scientifico, Università Ca' Foscari Venezia, 30172, Venezia, Mestre, Italy
[g] Dipartimento di Matematica e Geoscienze, Università di Trieste, Via E. Weiss 2, 34128, Trieste, Italy
[h] Istituto Nazionale di Oceanografia e di Geofisica Sperimentale (OGS), Borgo Grotta Gigante 42/c, I-34010, Sgonico, TS, Italy

A B S T R A C T

We present the results of the tephrochronology study of a 14.49 m long marine sediment core (TR 17–08) collected in the Edisto Inlet, Ross Sea (Antarctica). The core contains four cryptotephra layers at 55–56, 512–513, 517–518, and 524–525 cm of depth, which have been characterised by a detailed description of the texture, mineral assemblage, and single glass shards major and trace element geochemistry. The age model of the investigated sedimentary sequence, based on radiocarbon dating, indicates that the topmost cryptotephra correlates with the widespread 1254 CE tephra erupted by a historical eruption (696 ± 2 cal yrs BP) of Mount Rittmann, in northern Victoria Land. Deeper cryptotephra layers were derived from previously unknown explosive eruptions of Mount Melbourne volcano and were emplaced between 1615 cal yrs BP and 1677 cal yrs BP, e.g. between the 3rd and 4th centuries CE. This discovery demonstrates that the Mount Melbourne volcanic complex has been highly active in historical times allowing significant progress in the current understanding of regional eruptive history. Moreover, from a tephrochronological point of view, the detected cryptotephra provide new regional isochron markers to facilitate high-precision correlations and help stratigraphically constrain changes in environmental and climatic conditions that are identified by multidisciplinary studies.

1. Introduction

Explosive volcanic eruptions produce large volumes of mostly ash-sized pyroclastic products that can be transported in the atmosphere and rapidly sedimented across different depositional environments, over vast areas. The resulting tephra and cryptotephra (i.e. layers of volcanic ash not visible to the naked eye) layers are ideal as chronostratigraphic marker horizons but are at the same time important tools in volcanology and other disciplines of the Earth sciences like anthropology, archaeology, and pedology (Freundt et al., 2021 and references therein). The volcanological relevance of distal tephra and cryptotephra is enhanced in those settings, like Antarctica, where proximal exposures of volcanic rocks are scarce. In Antarctica, a special mention should be made to marine tephra layers that in the last years proved crucial to improve the knowledge of volcanic activity as well as for chronostratigraphic tools (Del Carlo et al., 2015; Di Roberto et al., 2019, 2020, 2021; Hillenbrand et al., 2008; Moreton and Smellie, 1998; Wilch et al., 1999). Antarctic marine tephra layers helped determine the style, magnitude, and intensity of past, previously unknown large explosive eruptions and their age (Di Vincenzo et al., 2010; Di Roberto et al., 2012; 2020, 2021). They also offered temporal and spatial correlations between ice and marine successions (Di Roberto et al., 2019; Wilch et al., 1999) that are of fundamental importance in the study of connections and coupling processes between atmospheric, ice sheets, ocean dynamics, and climate change. Volcanic ash is also part of the atmospheric dust that is distributed by atmospheric currents at different levels and depends on

* Corresponding author.
E-mail address: alessio.diroberto@ingv.it (A. Di Roberto).

https://doi.org/10.1016/j.qsa.2023.100079
Received 12 December 2022; Received in revised form 30 January 2023; Accepted 10 February 2023
Available online 18 February 2023

temporal variabilities. Therefore, volcanic ash distribution and trajectories during an eruption can be proxies of past wind circulation patterns.

Here we report the results of a tephrochronology study of the 14.49 m-long TR17-08 sediment piston core recovered from the Edisto Inlet, in the western Ross Sea, Antarctica, using magnetic, X-ray diffraction, textural, and geochemical analyses plus ten radiocarbon dates were acquired. Within the stratigraphic sequence, we detected four cryptotephra horizons, which were analysed in detail for the texture of volcanic fragments, major and trace element geochemistry, and mineral assemblage. Ten radiocarbon dating performed on carbonate material provided the core age model and tephra chronology. The results of our work indicate that tephra originated from historical eruptions of Mount Rittmann and Mount Melbourne volcanoes, located in northern Victoria Land, Antarctica.

We correlate the uppermost cryptotephra with the 1254 C.E. tephra from Mount Rittmann, representing a ubiquitous chronostratigraphic marker horizon for the marine and continental ice record of East and West Antarctica. Deeper in the sequence, we found three cryptotephra layers that can be associated, based on correlation with geochemical composition and age determinations, with historical explosive eruptions of Mount Melbourne.

Results contribute to constraining the rates of volcanism from two very active volcanic complexes of North Victoria Land and to adding new tephra isochrones available for tephrochronological purposes.

2. Study area

The Edisto Inlet is a small ice-filled fjord elongated in the NNE-SSW direction and situated between Cape Hallett and the North Victoria land coast, in the western Ross Sea, Antarctica (Fig. 1). It is approximately 15 km long and 4 km wide, and reaches a maximum water depth >500 m with a saddle 400 m-deep that separates the fjord from Moubray Bay to the north. Several small glaciers flow into the Edisto inlet and in particular the Manhaul Glacier in the west, and Edisto and Arneb glaciers in the south and east, respectively (Fig. 1). Sediment cores and geophysical data (3.5 kHz sub-bottom profiler) acquired near the fjord entrance during the 2002 and 2005 Programma Nazionale di Ricerche in Antartide (PNRA) Italian expeditions revealed that the inlet is characterised by a broadly flat seafloor morphology (Morelli et al., 2008) and by soft biogenic laminated sediments (Tesi et al., 2020).

3. Materials and methods

The piston core TR17-08 (72° 18.2778′ S; 170° 04.1784′ E; 462 m water depth) was collected (Fig. 1), during the XXXII PNRA Expedition (2016–2017), onboard the R/V Italica in the framework of the TRACERS project (PNRA16_00055). The 14.49 m-long core was divided into 1 m-long sections, stored at 4 °C on the vessel, and transported to the laboratories of CNR-ISMAR of Bologna.

The sediment core was measured for Magnetic Susceptibility (MS), X-rayed, opened in two halves, and described for lithology. The sediment comprises mainly laminated diatom ooze characterised by the alternation of light and dark laminae on the mm-to cm-scale throughout the core. According to the previous studies of cores from the same area, the lamination corresponds to several bloom cycles of diatom species (Finocchiaro et al., 2005; Mezgec et al., 2017; Tesi et al., 2020). This kind of sediment is the ideal archive for tephra and cryptotephra preservation as unaffected by consistent erosion or bioturbation.

3.1. Samples preparation and textural analyses

A third-generation AVAATECH core scanner with which high-resolution images and X-ray fluorescence (XRF) data were acquired for analyses at a 1 cm depth resolution.

Samples corresponding associated with indicative features

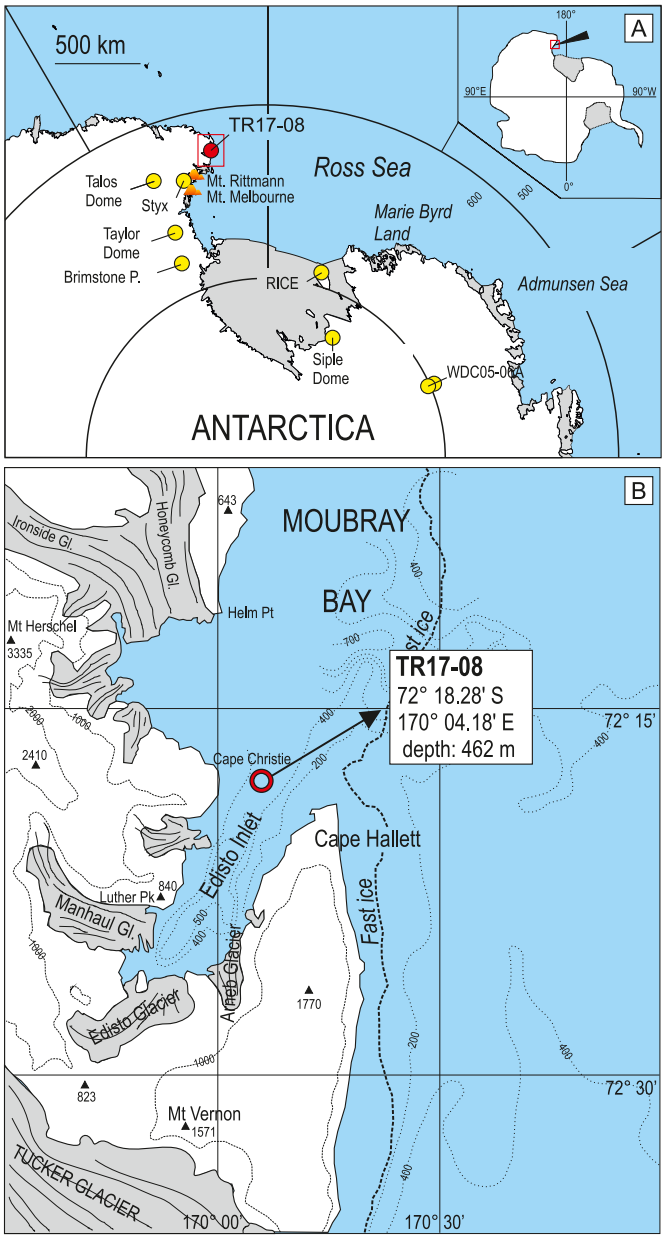

Fig. 1. Maps of the study area. a) Map of Antarctica showing the locations of the studied sediment core, ice core tephra archives, and blue ice field. b) Detail of the Edisto Inlet area and location of core TR17-08. Bathymetry and land morphology are from map SS 58–60/2 (Cape Hallett), original scale 1:250,000 edited by U.S. Geological Survey. Modified after Di Roberto et al. (2019). (For interpretation of the references to colour in this figure legend, the reader is referred to the Web version of this article.)

evidenced by XRF core scanning data (Fig. 2) were examined under a microscope to test the presence of volcanic particles (e.g., small fragments of pumice or scoria, glass shard, or magmatic crystals). We tested the presence of volcanic particles also in sediments respectively 1 cm above and 1 cm below the XRF anomalies. The samples showing the presence of volcanic particles were treated using hydrogen peroxide (H_2O_2) with 40% concentration to dissolve organic matter and washed with deionized water in an ultrasonic bath. Treated samples were sieved with a metal sieve with 0.032 mm (5 φ) mesh size ($\varphi = -\log_2 D$ with D = diameter of the particle or grain in millimetres), and dried at 60 °C. The samples were then prepared in 1-inch epoxy resin stubs, polished, and prepared for textural, mineralogical, and geochemical analyses. The textures of glass particles and the mineral phases composition were

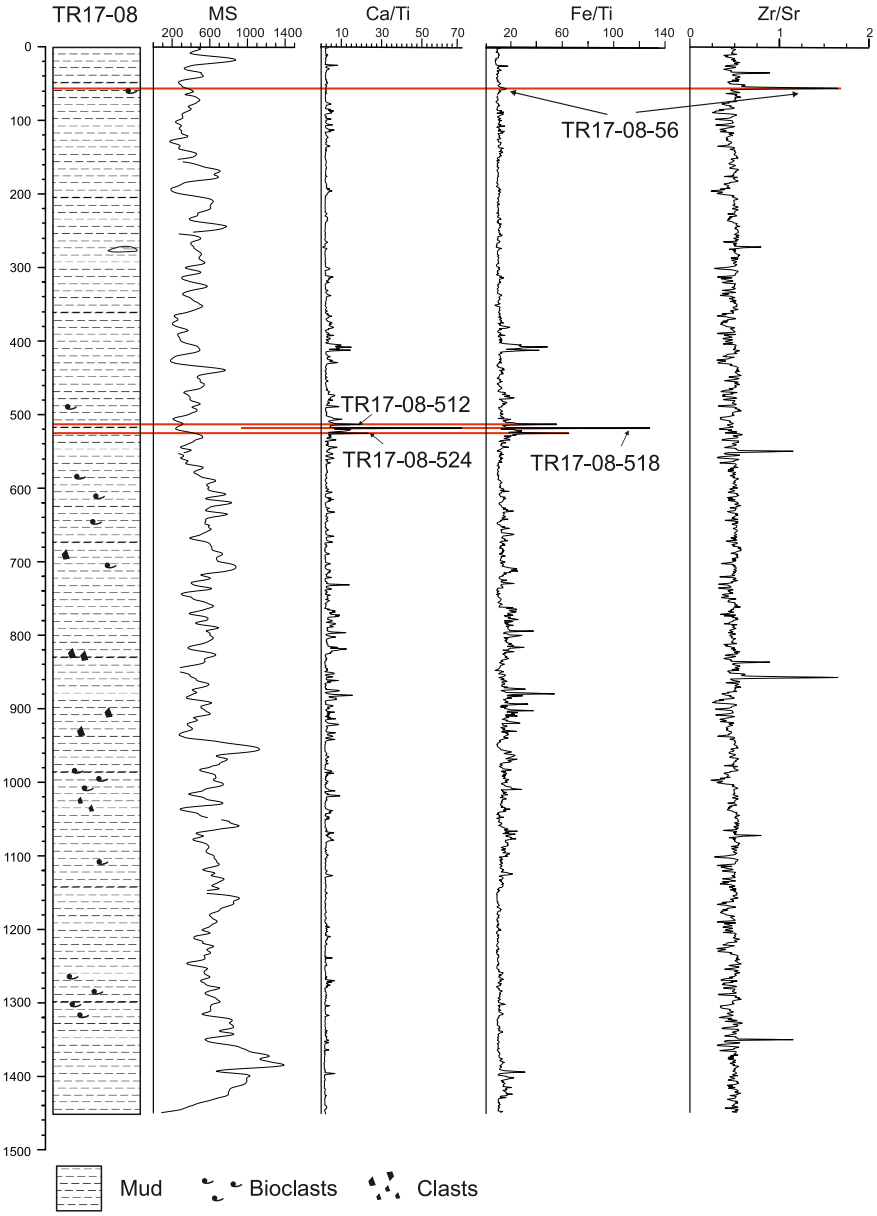

Fig. 2. Lithology, magnetic susceptibility curve, and XRF representative data (element ratios) for Core TR17-08. Red lines show the position of TR17-08-56 and TR17-08-512, −518, and −524 cryptotephra layers. (For interpretation of the references to colour in this figure legend, the reader is referred to the Web version of this article.)

studied at the Istituto Nazionale di Geofisica e Vulcanologia, Sezione di Pisa (INGV-Pisa) using a scanning electron microscope (SEM), Zeiss EVO MA equipped with an Oxford Energy-Dispersive X-Ray Spectroscopy system (EDS).

3.2. Major and trace elements composition

Major and minor element glass composition was determined using a JEOL JXA-8200 electron microprobe (EPMA) equipped with five wavelength-dispersive spectrometers at the High-Pressure High-Temperature (HPHT) Laboratory of INGV-Rome. Operating conditions were 15 kV accelerating voltage, 8 nA beam current, 5 mm probe diameter, and 10 and 5s acquisition time for peak and background, respectively). At least 30 single glass shards were analysed but compositions with a total oxide weight lower than 95% were discarded (Hunt and Hill, 1993).

The trace element compositions of glass shards were determined by laser ablation inductively coupled plasma mass spectrometry (LA-ICP-MS) at the Department of Physics and Geology, University of Perugia (Italy). The analyses were performed with a Teledyne Photon Machine G2 laser ablation system coupled with a Thermo Fisher Scientific iCAP-Q quadrupole-based ICP-MS (Petrelli et al., 2016a, 2016b). The operating conditions were optimised by analysing reference material NIST SRM 612 (Pearce et al., 1997) to provide maximum signal intensity and stability for the ions of interest while suppressing oxides formation (ThO+/Th + below 0.5%). The U/Th ratio was also monitored and maintained close to 1. The stability of the system was evaluated on ^{139}La, ^{208}Pb, ^{232}Th, and ^{238}U by a short-term stability test. It consisted of 5 acquisitions (1 min each) on a linear scan of NIST SRM 612 glass reference material (Petrelli et al., 2016a, 2016b). Tephra glasses were analysed by using a circular laser beam with a diameter of 20 μm, a frequency of 10 Hz, and an energy density at the sample surface of 3.5

J/cm^2. NIST SRM 610 (Pearce et al., 1997) reference material was used as the calibrator and ^{29}Si as the internal standard. USGS BCR2G reference material was analysed as unknown to provide quality control (Jochum et al., 2006; Supplemental Table 2). Under these operating conditions, precision and accuracy are better than 10% for all the investigated elements (Petrelli et al., 2016a, 2016b).

The glass compositions of the studied cryptotephra were compared with glass composition data available in the literature (Del Carlo et al., 2018) and a database of major- and trace-element compositions of Neogene-Quaternary tephra from Antarctic ice cores, marine sediments, and blue ice and continental outcrops (AntT database - https://www.tephrochronology.org/AntT/database.html). Major oxide and trace element compositions including reference standards are presented in Supplementary Tables 1 and 2

3.3. Multivariate statistics

Principal component analysis (PCA) is a multivariate statistical method that aims to exert relevant information from a data set and represent it in a lower-dimensional space (Jolliffe and Cadima, 2016). In detail, it extracts new uncorrelated variables from the data set, named principal components, that maximize variance (Jolliffe and Cadima, 2016). The main objective is to increase the interpretability of a data set by reducing the dimensionality of the problem but, at the same time, minimizing information loss (Jolliffe and Cadima, 2016).

The Principal Component Analysis (PCA) has been utilised to visualise trace element data (Rb, Sr, Y, Zr, Nb, Ba, La, Ce, Pr, Nd, Sm, Eu, Gd, Dy, Er, Yb, Lu, Hf, Ta, Pb, Th, and U), in a lower dimensional space. The compositional nature of chemical analyses has been accounted for by applying the centred log-ratio transformation (*clr*; Aitchison, 1986). It consists of dividing each chemical analysis for a specific element (e.g, Rb or Sr) by the geometric mean of all the determinations for that element, then making the logarithm (Aitchison, 1986):

$$clr(x) = \left[\ln\frac{x_1}{g(x)}, \ln\frac{x_2}{g(x)}, \ldots, \ln\frac{x_n}{g(x)}\right]$$

where $g(x)$ is the geometric mean of the element x.

3.4. Radiocarbon chronology

The Edisto Inlet is characterised by a very high sedimentation rate (ca. 0.55 cm/yr; Tesi et al., 2020) thus the age of tephra layers falls within the late Holocene. Moreover, since the studied cryptotephra bear few feldspar crystals and of very small size <200 μm (see text below), it was not possible to determine the tephra age directly (e.g., ^{40}Ar/^{39}Ar method). Consequently, the age model for the TR17-08 marine core and the age of cryptotephra layers rely on the radiocarbon dating of carbonate material (Table 1). Overall, we analysed ten samples, six ^{14}C ages throughout the core and four within cryptotephra. Analyses were performed at the MICADAS (Mini Carbon Dating System) of the Alfred-Wegener-Institut Helmholtz-Zentrum Für Polar-Und Meeresforschunglab. The ages were calibrated using the Marine13 curve (Reimer et al., 2013) and calibrated using a local reservoir correction (ΔR) of 790 ± 125 yrs (data from Hall et al., 2010 and adjusted to the new Intcal20 curve). We used the Marine13 curve instead of the latest Marine20 since the latter is not recommended in polar regions (Heaton et al., 2020). Ages across the record were obtained using OxCal4.4 using the P_Sequence deposition procedure and a *k* value (i.e., the index that sets the stiffness of the age-depth model upon the dating sequence) of 0.5 cm^{-1}. The OxCal age-depth model ran with Outlier-Model analysis using the General setting and a prior probability of 0.05, which weighs down the chronological constraints that have a probability >5% of being age reversals. No outliers were detected and a robust and coherent age model was generated with a high agreement index.

4. Results

4.1. Tephra components and texture

We identified cryptotephra at 55–56, 512–513, 517–518, and 524–525 cm of depth in core TR17-08 (herein after TR17-08-56, −512, −518, −524 tephra), respectively (Fig. 2). These correspond to relevant and sharp geochemical signals (spikes) in XRF data (e.g., Zr/Rb, Zr/Sr, Ti/Ca and Ti/K ratio in Fig. 2). Note that all sediment intervals corresponding to anomalies in the XRF data were inspected with the light stereomicroscope.

TR17-08-56 tephra consist of well-sorted, colourless to light-green glass shards and vesicular fragments up to 200 μm (red arrows in Fig. 3a) and scoriaceous, microlite-rich fragments up to 700 μm (blue

Table 1
Radiometric ages produced from TR17-08 sediment cores.

Name	Carbon source	Mean depth (cm)	Unmodelled (y BP)			Modelled (y BP)		
			median	from (2s)	to (2s)	median	from (2s)	to (2s)
dates used for the age-depth models								
Mt. Rittman tephra (687 ± 7 BP, WAIS chronology)*		55.5	687	701	673	687	702	672
TR17-08_XV_61-63	Echinoidea	62	801	1051	556	692	791	667
TR17-08_XIII_78-79	Echinoidea	234.5	1075	1310	790	1052	1263	862
TR17-08_X_13-14	Ophiuroidea	463.5	1416	1708	1157	1490	1684	1290
TR17-08_X_61-63	Foraminiferida (benthic)	512	1374	1721	1036	1612	1801	1420
TR17-08_X_66-69	Foraminiferida (benthic)	517.5	1743	2095	1395	1648	1832	1483
TR17-08_X_74-75	Foraminiferida (benthic)	524.5	1770	2116	1414	1677	1997	1518
TR17-08_X_75-76	Foraminiferida (benthic)	525.5	1782	2130	1421	1683	1997	1521
TR17-08_VIII_77-78	Ophiuroidea	729.5	2242	2640	1922	2219	2476	1971
TR17-08_VI_12-13	Echinoidea	863.5	2621	2922	2314	2527	2774	2309
TR17-08_I_17-18	Scaphopoda	1369.5	3376	3691	3035	3440	3760	3139
extrapolated ages for cryptotephras								
TR17-08-512		512.5				1615	1804	1424
TR17-08-518		517.5				1648	1832	1483
TR17-08-524		524.5				1677	1997	1518

*Narcisi, B., Petit, J. R. & Chappellaz, J. 2010. A 70 ka record of explosive eruptions from the TALDICE ice core (Talos Dome, East Antarctic plateau). J. Quat. Sci. 25, 844–849 (2010); Iverson, N. A. Characterization and correlation of englacial tephra from blue ice areas and ice cores, Antarctica Nels Anton Iverson Dissertation Submitted as Partial Fulfillment of the Requirements for the Degree of Doctor of Philosophy in Earth and Environmental Sc (2017).

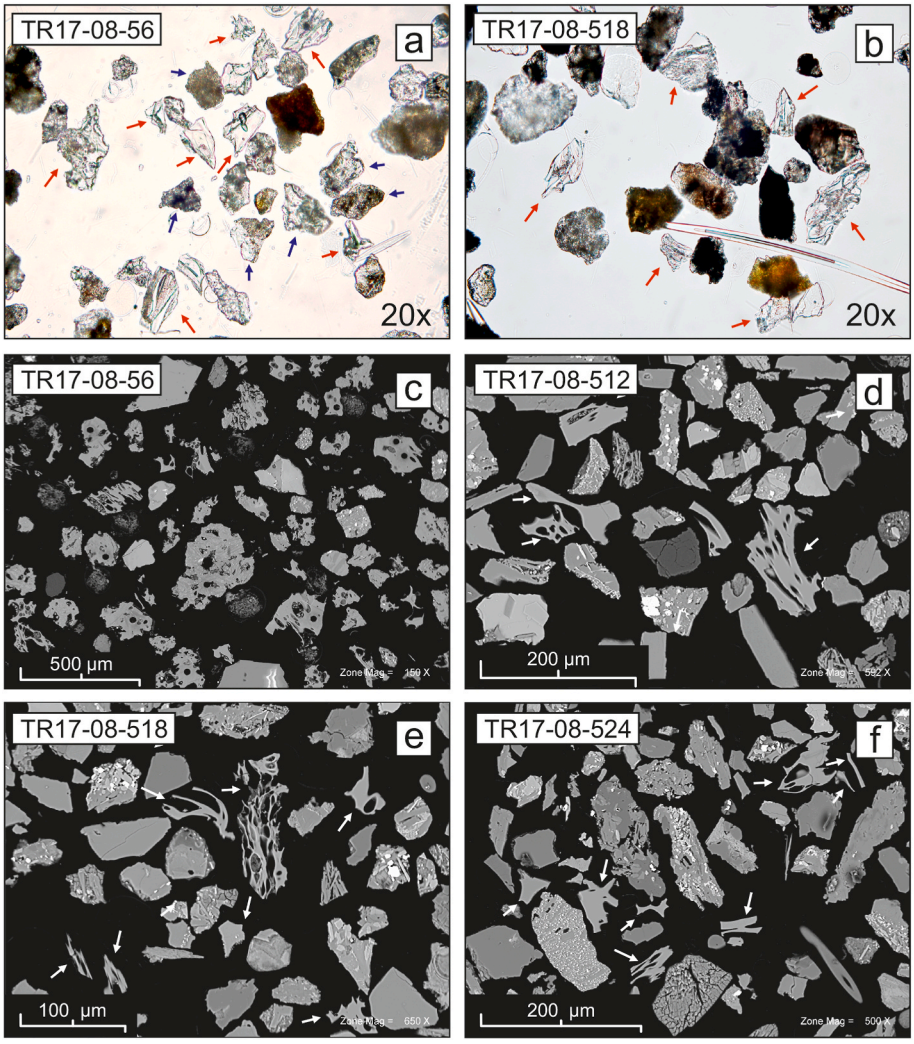

Fig. 3. Light microscope and scanning electron microscope (SEM) backscatter images of particles forming the cryptotephra layers found in the TR17-08 core. a) light microscope image of TR17-08-56 cryptotephra deriving from the 1254 CE eruption of Mount Rittmann. Particles include aphyric to microlite poor, vesicular glass shards (red arrows) and microlites-rich (K-feldspar, plagioclase, and Fe–Ti spinels) scoria fragments (blue arrows). b) light microscope image of TR17-08-518 cryptotephra from Mount Melbourne. Red arrows indicate aphyric, vesicular glass shards forming the cryptotephra layers dispersed in the volcanoclastic sediment. c) SEM backscatter images of TR17-08-56 cryptotephra from Mount Rittmann, d-f) SEM backscatter images of d - TR17-08-512; e – TR17-08-518 and f - TR17-08-524 cryptotephra layers showing glass shards morphologies. (For interpretation of the references to colour in this figure legend, the reader is referred to the Web version of this article.)

arrows in Fig. 3a). Glass shards are aphyric to microlite poor and occur in multiple morphologies including blocky, cuspate, y-shaped, or platy glass (Fig. 3a, c), and vesicular fragments are moderate to high vesicular and range texturally from frothy-vesicular to tubular (Fig. 3a, c). Light brown to dark brown scoria fragments are also present (Fig. 3a, c); the latter is rich in acicular microlites of K-feldspar, plagioclase, and Fe–Ti spinels (Fig. 3a). Crystals of feldspars and clinopyroxene up to 200 μm rimmed with volcanic glass also occur. Few lithic fragments comprise sideromelane faintly altered to palagonite and holocrystalline volcanic rocks (Fig. 3a, c).

TR17-08-512, −518, and −524 cryptotephra, respectively are characterised by very similar particle texture and components, even with slight variation in the particle type relative abundance. Cryptotephra particles (red arrows in Fig. 3b and white arrows of Fig. 3d–f) comprise colourless to light-green glass shards up to 100 μm and pumices fragments up to 150 μm (Fig. 3b), respectively, which are embedded in volcaniclastic sediment. Glass shards are mostly crystal-free and have a blocky, y-shaped and bubble wall morphology (Fig. 3d–e). The pumice fragments are moderate vesicular and range texturally from frothy-vesicular to tubular (Fig. 3d–e). Shards preserve fragile glass tips and show no abrasion or rounding. Glass is usually aphyric but rare fragments bearing acicular plagioclase, clinopyroxene, and oxide microliths occur.

4.2. Major and trace elements composition

Glass compositions of the cryptotephra corresponding to the TR17-08-56 sample are predominantly trachytic. A few compositions plot across the boundary with phonolites in the total alkalis-silica diagram (TAS; LeBas et al., 1986, Fig. 4a). Average total alkalis value is 13.1 wt % ($2\sigma = 0.35$) and the average K_2O/Na_2O ratio is 0.64 ($2\sigma = 0.03$). Mean CaO and FeO contents are ~1 wt % ($2\sigma = 0.1$) and ~6.4 wt % ($2\sigma = 0.14$), respectively (Fig. 5; Table 2). Trace element distributions for TR17-02-56 tephra are reported in the spidergram of Fig. 4b. The trace element compositions of the TR17-02-56 cryptotephra are enriched compared to PM (Primitive Mantle; McDonough and Sun, 1995) values for most of the investigated elements (i.e., from ~10x to ~200x). Glasses composition normalised to the PM displays prominent negative anomalies in Ba, Sr, and Ti which may be related to the fractionation of alkali feldspar, plagioclase, and oxides (Fig. 4b). These trachytes-phonolites are enriched with incompatible trace elements, for example, Zr is 500–849 ppm and Th is 9.5–19.6 ppm. High-Field-Strenght Elements (HFSE) ratios vs. Th remain fairly constant (Fig. 6), with Zr/Th = 47.26 ± 2.44, Nb/Th = 11.58 ± 0.59, and Y/Th = 3.95 ± 0.28.

Glass compositions of the TR17-08-512, −518, and −524 cryptotephra plot in a narrow cluster in the trachyte field of the TAS diagram (Fig. 4a). Mean total alkalis values range from 9.9 to 10.4 wt % and average K_2O/Na_2O ratios are between 0.87 and 0.92. Mean CaO and FeO contents are ~1.7 wt % ($2\sigma = 0.3$) and c. 5 wt% ($2\sigma = 0.6$), respectively (Fig. 5b and c). Trace element distributions for TR17-08-512, −518, and

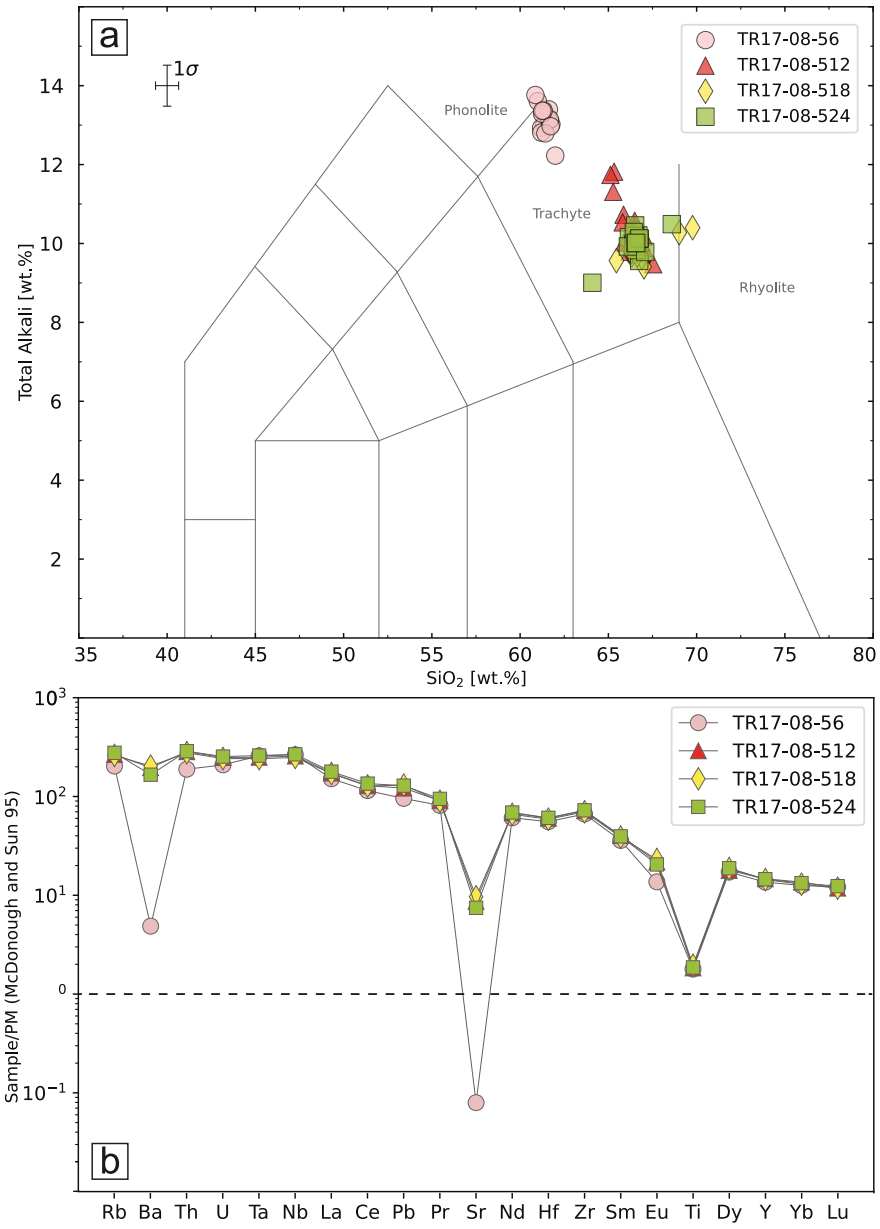

Fig. 4. a) Total Alkali *versus* Silica (TAS) classification diagram (LeBas et al., 1986) and (b) normalised spider diagram for primitive mantle (after McDonough and Sun, 1995) showing the glass major and trace element compositions (representative average value) of the tephra found in Edisto Inlet marine sequence.

−524 cryptotephra are reported in selected bi-plot variation diagrams of Fig. 6. Also, in this case, the trace element compositions of studied cryptotephra perfectly overlap and normalised to the PM, they display identical patterns with slight negative anomalies in Sr and Ti (Fig. 4b) which may be related to the fractionation of plagioclase and oxides. Light Rare Earth Elements (LREE) are enriched relative to Heavy Rare Earth Elements (HREE). These trachytes are significantly enriched in incompatible elements, e.g., Zr is 607–856 ppm and Th 19.5–26.7 ppm. HFSE ratios vs. Th remain constant (Fig. 6) with Zr/Th = 33.74 ± 3.3, Nb/Th = 7.63 ± 1.05, and Y/Th = 2.81 ± 0.29.

4.3. Age-depth models and age of cryptotephras

According to our age-depth model, the TR17-08 core encompasses the last 3400 years BP (Fig. 7). The age of Mount Rittman tephra, also known as 1254 C.E. tephra (TR17-02-56) is 687 ± 7 BP, and is derived by West Antarctic Ice Sheets chronology (Narcisi et al., 2010; Iverson, 2017).

Down in the core, within the interval that contains cryptotephras (TR17-08-512, TR17-08-518, and TR17-08-524), ages extrapolated from the age-depth model are 1615 yrs cal. BP (1804-1424 yrs BP; 2σ), 1648 yrs cal. BP (1832-1483 yrs cal. BP; 2σ) and 1677 yrs cal. BP (1997-1518 yrs cal. BP; 2σ), respectively. The ages of the identified cryptotephra layers indicate that their respective eruptions occurred within a short time interval.

5. Discussion

5.1. Tephra emplacement

The Edisto Inlet is ice-bound for much of the year apart from a few weeks in late summer/early winter. Tephra and cryptotephra found in the Edisto Inlet's marine sediment could be deposited directly through the water column in the short ice-free window, or deposited first on sea

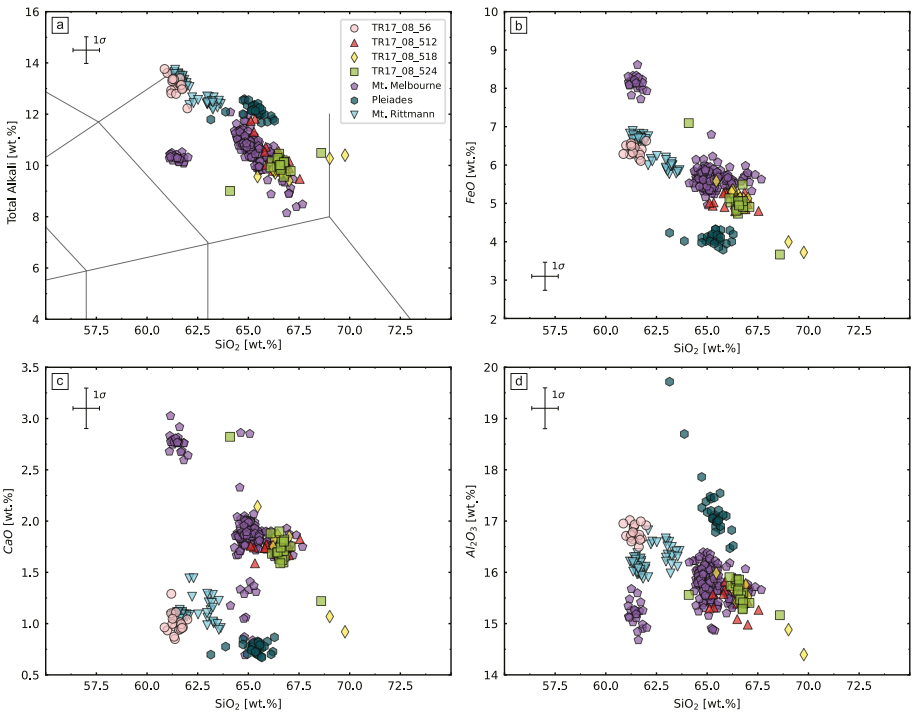

Fig. 5. a) TAS classification diagram (LeBas et al., 1986) and (b-d) major element bivariate plot showing glass compositions of the tephra samples found in Edisto Inlet marine sequence compared to glass major element composition of proximal volcanic deposits of northern Victoria Land volcanoes including Mount Melbourne, Mount Rittmann and The Pleiades. All data are normalised to a 100% total. Reference tephra data used for comparison are from Del Carlo et al. (2022); Lee et al. (2019). Mount Rittmann: Di Roberto et al. (2019, 2020); Lee et al. (2019). The Pleiades: Lee et al. (2019); this work.

Table 2
Average chemical composition of cryptotephra found in core TR17-08.

	TR17–08–56		TR17–08–512		TR17–08–518		TR17–08–524	
	Average (n = 18)	st.dev	Average (n = 20)	st.dev	Average (n = 20)	st.dev	Average (n = 20)	st.dev
SiO2	61.42	0.29	66.34	0.65	66.76	0.96	66.57	0.77
Al2O3	16.78	0.15	15.52	0.25	15.55	0.35	15.59	0.22
FeO	6.39	0.14	5.03	0.18	4.99	0.43	5.03	0.59
TiO2	0.41	0.08	0.39	0.06	0.41	0.09	0.40	0.07
P2O5	0.07	0.03	0.05	0.03	0.05	0.03	0.07	0.05
CaO	1.00	0.10	1.73	0.06	1.69	0.26	1.75	0.29
MgO	0.18	0.05	0.17	0.04	0.17	0.06	0.17	0.04
MnO	0.18	0.04	0.10	0.03	0.10	0.03	0.11	0.02
Na2O	7.99	0.34	5.56	0.65	5.18	0.18	5.22	0.22
K2O	5.14	0.11	4.77	0.13	4.77	0.17	4.80	0.24
F	0.19	0.03	0.15	0.03	0.15	0.02	0.13	0.03
Cl	0.26	0.03	0.18	0.02	0.19	0.04	0.18	0.02
Alkali	13.14	0.35	10.32	0.67	9.94	0.27	10.01	0.32
K2O/Na2O	0.64	0.03	0.87	0.09	0.92	0.04	0.92	0.06

ice and then redeposited during the melting of sea ice.

The TR17-08-56 cryptotephra shows features that suggest a primary deposition through the water column. The layer is characterised by a well-sorted grainsize, has a homogeneous geochemical composition, contains rare volcaniclastic or detrital particles and glass shards show pristine shape, indicating no to a very low degree of transport. TR17-08-512, 518 and 524 cryptotephra have similar features but are characterised by a lower abundance of glass shards dispersed within volcaniclastic sediment, which might support the hypothesis that they first deposited on the sea-ice, and then redeposited after sea ice melting. Even in the case of a secondary transport, given the very short interval between the eruptions and the final deposition (at most in the order of a few months), the studied cryptotephra layers would not lose their value as potential tephrochronological and stratigraphic markers. As described by Di Roberto et al. (2019), the Edisto Inlet sediment sequences comprise very expanded Holocene sediments almost entirely made by soft biogenic (diatomaceous ooze) laminated sediments without evidence for relevant ice-rafted debris input, especially in the sediment interval where the cryptotephra is contained. Thus, the sedimentation via iceberg rafting for the studied cryptotephra, which could explain the abundance of volcaniclastic components, can reasonably be ruled out.

5.2. *Source correlation and tephra dispersal*

The volcanoes of the South Sandwich Islands, as well as the intraplate Antarctic volcanoes of Marie Byrd Land and Victoria Land, represent the main sources of tephra recognized in the different records of Antarctica (Narcisi et al., 2012; Di Roberto et al., 2019, 2021; Hopfenblatt et al., 2022). Extra-Antarctic sources, with particular reference to the South America and New Zealand volcanoes, have been also suggested (Narcisi et al., 2012) but most of the correlations proposed are weakly constrained (Del Carlo et al., 2018). The only confirmed extra-Antarctic tephra that was identified in ice-core records is attributed to the c. 25.6 kyr Oruanui super-eruption from Taupo volcano (Dunbar et al., 2017). Recently, the presence of a cryptotephra from a peat section on sub-Antarctic South Georgia was also confirmed and a correlation with the 2950 cal yrs BP Alpehué eruption of the Chilean

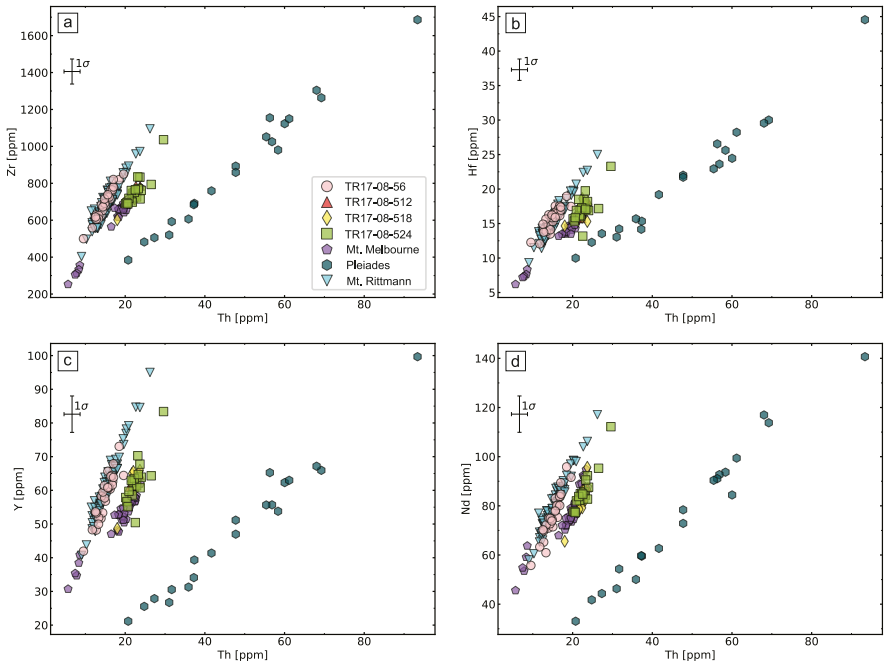

Fig. 6. Bivariate plots of trace elements glass composition of the tephra layers found in Edisto Inlet marine sequence compared to glass trace element composition from proximal volcanic deposits of northern Victoria Land volcanoes including Mount Melbourne, Mount Rittmann, and The Pleiades. Data used for comparison are from: Mount Melbourne: Del Carlo et al. (2022); Lee et al. (2019); Mount Rittmann: Di Roberto et al. (2019, 2020); Lee et al. (2019). The Pleiades: Lee et al. (2019); this work.

Sollipulli volcano was proposed (Oppedal et al., 2018). In addition, extremely fine ashes (<5 μm) found in surface snow and shallow firn samples, were attributed to the 2011 eruption of Puyehue-Cordón Caulle (Chile (Koffman et al., 2017); and the 1257 CE Samalas eruption, in Indonesia (Narcisi et al., 2019). However, this last attribution is based on electron microprobe geochemical data showing a very low total oxide weight percentage (down to 60 wt%), obtained on extremely small particles (a few microns), and cannot be confirmed. Note that analyses of volcanic glass with a total oxide weight lower than 95% should be discarded (Hunt and Hill, 1993).

The average grain size of particles in the studied cryptotephra (around 100 μm) suggests a source located in Antarctica, not too far from the sampling site. The Na-alkaline phonolitic-trachytic and trachytic compositions point toward the intraplate alkaline volcanoes of the McMurdo Volcanic Group in Victoria Land as possible sources rather than the low-alkali tholeiitic South Sandwich Islands and calc-alkaline South Shetland volcanoes. We thus compared the glass composition of the studied tephra with the glass composition of tephra samples recovered on proximal exposure of McMurdo Volcanic Group in Victoria Land as well as with the composition of distal tephra found in ice cores.

The major and trace element glass compositions of TR17-08-56 cryptotephra plot in the compositional field of products of Mount Rittmann volcano (Fig. 5; Di Roberto et al., 2019; Lee et al., 2019). In particular, the glass composition of TR17-08-56 cryptotephra matches both that of proximal deposits sampled on top of Mount Rittmann (Di Roberto et al., 2019, 2020) and of cryptotephra layers found at 139–140 cm of depth in core BAY05-c20 (Di Roberto et al., 2019) and 136.5 cm of depth in the HLF17-1 core (Tesi et al., 2020), both recovered in the Edisto Inlet. These distal tephra have been in turn correlated with the widespread 1254 CE trachytic tephra attributed to Mount Rittmann and also found in deep ice cores at Taylor Dome (Dunbar et al., 2003), Siple Dome and Talos Dome (Dunbar and Kurbatov, 2011; Narcisi et al., 2012, 2017) and several shallow ice cores in East and West Antarctica (Han et al., 2015; Iverson, 2017).

Multivariate statistical investigations, i.e., PCA analysis, further support the hypothesis that Mount Rittmann volcano is the volcanic source for the TR17-08-56 cryptotephra (Fig. 8). In detail, the PCA on trace elements (Fig. 8a, c) allows the discrimination among Mt. Melbourne, Pleiades, and Mt. Rittman proximal samples and the attribution of each unknown sample (i.e., TR17-08-56, TR17-08-512, TR17-08-518, and TR17-08-524) to a specific volcanic source. To better understand the role of each trace element in the modulation of the different PCs, Fig. 8d–e shows the relative contribution of these elements in the PC2 vs PC1 (Fig. 8a) and PC3 vs PC2 (Fig. 8b), respectively. Finally, Fig. 8f reports the cumulative explained variance of the PCA. In detail, Fig. 8F highlights that considering the PC1 alone, the explained variance is ~90%. Including PC2 and 3, the explained variance is ~94 and more than 95%, respectively.

It was proposed that the 1254 CE tephra derive from a long-lasting, ash-forming eruption of the Mount Rittman volcano that occurred c. 700 yrs BP (Di Roberto et al., 2019). This determination also helps define the age for the additional tephra layers down in the core, which clearly is older than c. 700 yrs BP.

The major and trace element glass compositions of the TR17-08-512, −518, and −524 cryptotephra fall within the compositional field of the proximal explosive products of Mount Melbourne (Figs. 4 and 5). A very good geochemical match exists with the major element composition of tephra sample A1621 from Mount Melbourne (Lee et al., 2019) c. 300 km from the Edisto Inlet. Conversely, there is no overlap with the composition of proximal trachytic products sampled on the summit of Mount Melbourne volcano recently reported by Del Carlo et al. (2022) and interpreted as the result of Strombolian to sub-Plinian/Plinian eruptions yielding ^{40}Ar-^{39}Ar ages younger than 13.5 ± 4.3 ky.

The glass compositions of studied cryptotephra have a c. 2 wt % higher average content of SiO_2 and slightly lower alkalis content (c. 1 wt %) relative to Mount Melbourne, along with other differences in the concentration of the other major oxides (Figs. 4 and 5). Trace element compositions of studied tephra layers are comparable with those of summit products of Mount Melbourne with slightly higher content in incompatible elements like for example Zr, Y, and La confirming the correlation to this volcanic source.

Searching for distal tephra correlation, we found that no direct match exists with the composition of tephra layers found in the younger part (<16 kyr) of the Talos Dome ice core, most of which have been previously attributed to Mount Melbourne (Narcisi et al., 2012), or with tephra in the Siple and Taylor ice cores (Dunbar et al., 2003). No

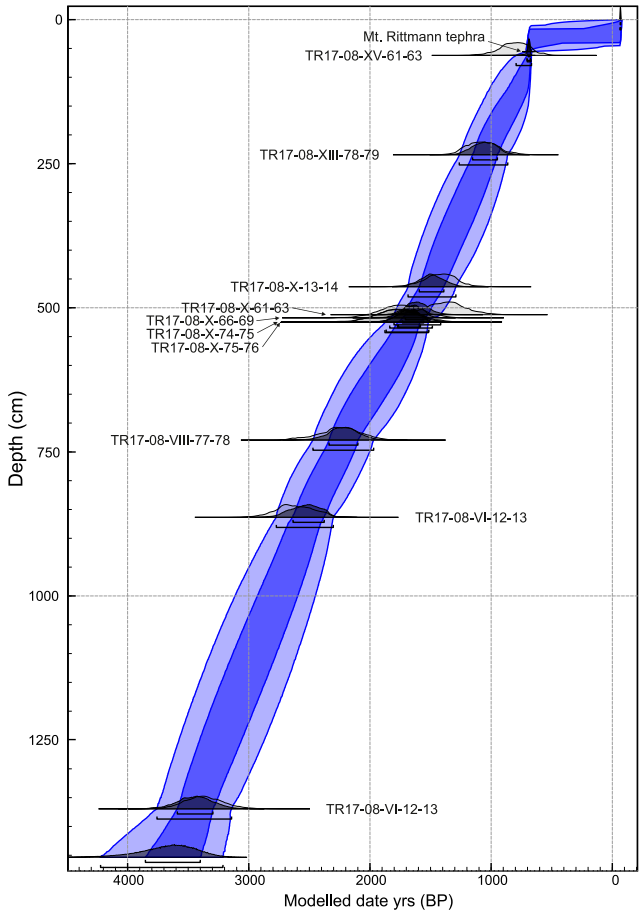

Fig. 7. Age-depth model for core TR17-08. The age model is constrained by ten calibrated radiocarbon dates; the lighter and darker blue shaded areas represent 95% and 65% confidence intervals of the modelled core chronology. Radiocarbon determinations were calibrated using OxCal. v4.4.4 (Bronk Ramsey, 2021) and the Marine 13 curve (Reimer et al., 2013). (For interpretation of the references to colour in this figure legend, the reader is referred to the Web version of this article.)

correlation exists with tephra found in Styx Glacier ice core records which is the record closer to the Mount Melbourne volcano but should date back only to c. 1.04 kyr (Han et al., 2015). The PCA also points to a strong affinity of the TR17-08-512, −518, and −524 cryptotephra with Mount Melbourne volcanics (Fig. 8).

In summary, we suggest that TR17-08-512, −518, and −524 cryptotephra derive from a series of explosive eruptions that occurred in a very short time interval (a few decades scale) from Mount Melbourne between 1615 cal yrs BP (1804-1424 cal yrs BP; 2σ), and 1677 cal yrs BP (1997-1518 cal yrs BP; 2σ), i.e., between the 3rd and 4th century CE. The fine ashes from these eruptions were dispersed mainly to the northeast, up to the Edisto Inlet c. 300 km from the source. These previously unknown eruptions likely took place from vents belonging to the Mount Melbourne volcanic field complex.

The obtained results emphasize that studies of tephra and cryptotephra layers allow significant progress in reconstructing regional volcanic histories. In detail, the marine cryptotephra of Edisto Inlet contributes to constraining the rates of volcanism from Mount Melbourne and indicates that this volcanic complex has been strongly active in historical times.

From a tephrochronological point of view *stricto sensu*, the wide areal dispersal of the studied tephra and cryptotephra layers found c. 300 km away from the volcanic source, allows cross correlation between the marine sediment of the Edisto Inlet and englacial sequences on the flank of Mount Melbourne and provides new chronostratigraphic marker beds to connect and synchronize geological and palaeoenvironmental event. Similarly to the Mount Rittmann 1254 CE tephra, these layers should be useful as additional points for precise dating and support the development of accurate age-depth models for sedimentary sequences in the Antarctic region.

The atmospheric cargo of dust (including fine volcanic ash particles) is distributed by currents at different levels and the dispersal depends on the temporal variabilities of these currents (Obreht et al., 2017; Plunkett et al., 2020). A generally persistent large-scale clockwise (westerly) circulation characterises the average Antarctic wind pattern both in the summer and winter seasons (Geyer et al., 2017). This circulation characterises all atmospheric levels including mid-troposphere, tropopause, and low-stratosphere, which mainly transport products of volcanic plumes (from eruptions of any size), and consequently controls the dispersal of eruption clouds and pyroclastic products.

Tephra input in the atmospheric load is punctual in time and space (Narcisi et al., 2005) and the distance reached by ash away from the source volcano depends on the height of the eruption column, the temperature of the air, and wind direction and speed. Information from modern atmospheric dynamics represent a proxy for palaeoatmospheric condition that would be responsible for the distribution of ash. Therefore, records of ash in ice and sediment cores that have known sources can be useful in identifying local, seasonal and periodical perturbation of the main atmospheric circulation model.

The dispersal of studied tephra from Mount Rittmann and Mount Melbourne to the Edisto Inlet is in agreement with and validates the results of the meteorological model over Antarctica proposed by Geyer et al. (2017). According to the result of the model (see Fig. 3 of Geyer et al., 2017), eruption columns between 5 and 10 km in height, from Mount Rittmann and Mount Melbourne volcanoes, would intercept winds with speeds between 10 and 30 m/s. Such winds would easily spread the volcanic plumes and carry tephras downwind for some hundreds of kilometres from the sources. In this case, field data validate the model results and in turn, the model suggests that the eruptions that deposited the studied tephras were characterised by eruptive plumes of considerable height, capable of reaching low-stratosphere.

6. Conclusions

Tephra layers preserved in distal archives have been demonstrated to be of pivotal importance to enhance the knowledge and understanding of the volcanic history of a region, especially when proximal volcanic successions are scarce as in the glacierized areas of Antarctica.

An integrated investigation performed on the piston core TR17-08 collected in the Edisto Inlet document that Mount Melbourne is an active volcano with a high-level of explosive activity in the 3rd-4th centuries CE. In fact, besides the historic eruption from Mount Rittman (1254 CE) that has been extensively documented in the literature, our research allowed us to detect three additional cryptotephra layers from Mount Melbourne at 1615 yrs cal. BP, 1648 yrs cal. BP and 1677 yrs cal. BP that were not previously known. These unprecedented data provide additional chronostratigraphic control points for the tephrostratigraphic studies in the Antarctic region. Moreover, the areal distribution and characteristics of identified tephra provide insight into the wind regime suggesting scenarios that are consistent with those proposed by numerical simulations. Besides information on the frequency of volcanic activity and styles of eruption, tephra can provide information that is relevant to paleoclimatic conditions in Antarctica.

Declaration of competing interest

The authors declare that they have no known competing financial interests or personal relationships that could have appeared to influence the work reported in this paper.

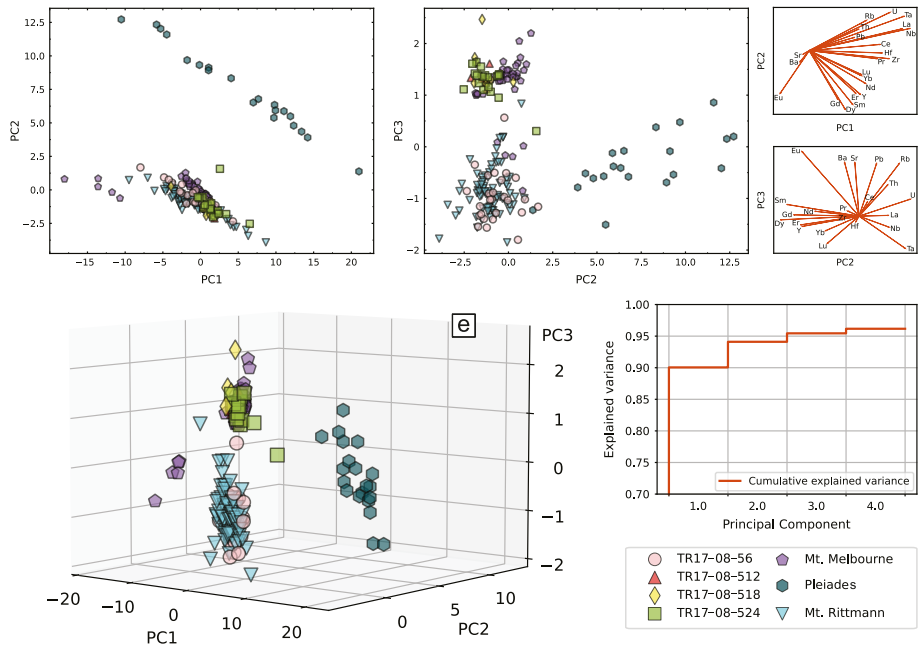

Fig. 8. Application of the Principal Component Analysis to trace elements data of tephra layers found in Edisto Inlet marine sequence and proximal volcanic deposits of northern Victoria Land volcanoes, i.e., Mount Melbourne, Mount Rittmann, and The Pleiades.

Data availability

data are included as Supplementary materials

Acknowledgements

This work was funded by Italian MIUR-PNRA program (Ministero dell'Università e della Ricerca - Programma Nazionale di Ricerche in Antartide) in the framework of TRACERS project (TephRochronology and mArker events for the CorrElation of natural archives in the Ross Sea, Antarctica; grant PNRA2016-A3/00055), CHIMERA project (CryptotepHra In Marine sEquences of the Ross Sea, Antarctica: implications and potential applications; grant PNRA18_00158-A), and EDISTHO project (Edisto inlet DIatom laminations Sequences Through the HOlocene; grant PNRA2018_00010).

This paper is sponsored by the SCAR (Scientific Committee on Antarctic Research) Expert Group, AntVolc.

Appendix A. Supplementary data

Supplementary data to this article can be found online at https://doi.org/10.1016/j.qsa.2023.100079.

References

Aitchison, J., 1986. The Statistical Analysis of Compositional Data. Monographs on Statistics and Applied Probability. Chapman & Hall Ltd, London.

Bronk Ramsey, C. 2021. OxCal. v 4.4.4. https://c14.arch.ox.ac.uk/oxcal.html.

Del Carlo, P., Di Roberto, A., Di Vincenzo, G., Bertagnini, A., Landi, P., Pompilio, M., Colizza, E., Giordano, G., 2015. Late Pleistocene-Holocene volcanic activity in northern Victoria Land recorded in Ross Sea (Antarctica) marine sediments. Bull. Volcanol. 77, 1–17. https://doi.org/10.1007/s00445-015-0924-0.

Del Carlo, P., Di Roberto, A., D'Orazio, M., Petrelli, M., Angioletti, A., Zanchetta, G., Maggi, V., Daga, R., Nazzari, M., Rocchi, S., 2018. Late Glacial-Holocene tephra from southern Patagonia and Tierra del Fuego (Argentina, Chile): a complete textural and geochemical fingerprinting for distal correlations in the Southern Hemisphere. Quat. Sci. Rev. 195, 153–170. https://doi.org/10.1016/j.quascirev.2018.07.028.

Del Carlo, P., Di Roberto, A., Di Vincenzo, G., Re, G., Albert, P.G., Nazzari, M., Smith, V. C., Cannata, A., 2022. Tephrostratigraphy of proximal pyroclastic sequences at Mount Melbourne (northern Victoria Land, Antarctica): insights into the volcanic activity since the last glacial period. J. Volcanol. Geoth. Res. 422, 107457 https://doi.org/10.1016/J.JVOLGEORES.2021.107457.

Di Roberto, A., Albert, P.G., Colizza, E., Del Carlo, P., Di Vincenzo, G., Gallerani, A., Giglio, F., Kuhn, G., Macrì, P., Manning, C.J., Melis, R., Miserocchi, S., Scateni, B., Smith, V.C., Torricella, F., Winkler, A., 2020. Evidence for a large-magnitude Holocene eruption of Mount Rittmann (Antarctica): a volcanological reconstruction using the marine tephra record. Quat. Sci. Rev. 250, 106629 https://doi.org/10.1016/j.quascirev.2020.106629.

Di Roberto, A., Colizza, E., Del Carlo, P., Petrelli, M., Finocchiaro, F., Kuhn, G., 2019. First marine cryptotephra in Antarctica found in sediments of the western Ross Sea correlates with englacial tephras and climate records. Sci. Rep. 9, 1–10. https://doi.org/10.1038/s41598-019-47188-3.

Di Roberto, A., Del Carlo, P., Pompilio, M., 2021a. Marine record of antarctic volcanism from drill cores. In: Geological Society Memoir. Geological Society of London, pp. 631–647. https://doi.org/10.1144/M55-2018-49.

Di Roberto, A., Del Carlo, P., Rocchi, S., Panter, K.S., 2012. Early Miocene volcanic activity and paleoenvironment conditions recorded in tephra layers of the AND-2A core (southern McMurdo Sound, Antarctica). Geosphere, 8 (6), 1342–1355. https://doi.org/10.1130/GES00754.1.

Di Roberto, A., Scateni, B., Di Vincenzo, G., Petrelli, M., Fisauli, G., Barker, S.J., Del Carlo, P., Colleoni, F., Kulhanek, D.K., McKay, R., De Santis, L., 2021b. Tephrochronology and provenance of an early pleistocene (calabrian) tephra from IODP expedition 374 site U1524, Ross Sea (Antarctica). G-cubed 22, 1–19. https://doi.org/10.1029/2021GC009739.

Dunbar, N.W., Kurbatov, A.V., 2011. Tephrochronology of the Siple Dome ice core, West Antarctica: correlations and sources. Quat. Sci. Rev. 30, 1602–1614. https://doi.org/10.1016/j.quascirev.2011.03.015.

Dunbar, N.W., Zielinski, G.A., Voisins, D.T., 2003. Tephra layers in the Siple Dome and taylor Dome ice cores, Antarctica: sources and correlations. J. Geophys. Res. 108, 2374. https://doi.org/10.1029/2002jb002056.

Di Vincenzo, G., Bracciali, L., Del Carlo, P., Panter, K., Rocchi, S., 2010. ^{40}Ar–^{39}Ar dating of volcanogenic products from the AND-2A core (ANDRILL Southern McMurdo Sound Project, Antarctica): correlations with the Erebus Volcanic Province and implications for the age model of the core. Bull. Volcanol. 72, 487–505. https://doi.org/10.1007/s00445-009-0337-z.

Dunbar, N.W., Iverson, N.A., Van Eaton, A.R., Sigl, M., Alloway, B.V., Kurbatov, A.V., Mastin, L.G., McConnell, J.R., Wilson, C.J.N., 2017. New Zealand supereruption provides time marker for the Last Glacial Maximum in Antarctica. Sci. Rep. 7, 12238 https://doi.org/10.1038/s41598-017-11758-0.

Finocchiaro, F., Langone, L., Colizza, E., Fontolan, G., Giglio, F., Tuzzi, E., 2005. Record of the early Holocene warming in a laminated sediment core from Cape Hallett Bay (northern Victoria land, Antarctica). Global Planet. Change 45, 193–206. https://doi.org/10.1016/j.gloplacha.2004.09.03.

Freundt, A., Schindlbeck-Belo, J.C., Kutterolf, S., Hopkins, J.L., 2021. Tephra layers in the marine environment: a review of properties and emplacement processes. Geol. Soc. London, Spec. Publ. 520 https://doi.org/10.1144/sp520-2021-50.

Geyer, A., Marti, A., Giralt, S., Folch, A., 2017. Potential ash impact from Antarctic volcanoes: insights from Deception Island's most recent eruption. Sci. Rep. 7, 16534 https://doi.org/10.1038/s41598-017-16630-9.

Hall, B.L., Henderson, G.M., Baroni, C., Kellogg, T.B., 2010. Constant Holocene Southern-Ocean 14C reservoir ages and ice-shelf flow rates. Earth Planet Sci. Lett. 296, 115e123. https://doi.org/10.1016/j.epsl.2010.04.054.

Han, Y., Jun, S.J., Miyahara, M., Lee, H.-G., Ahn, J., Chung, J.W., Hur, S. Do, Hong, S.B., 2015. Shallow ice-core drilling on Styx glacier, northern Victoria Land, Antarctica in the 2014-2015 summer. J. Geol. Soc. Korea 51, 343–356. https://doi.org/10.14770/jgsk.2015.51.3.343.

Heaton, T.J., Köhler, P., Butzin, M., Bard, E., Reimer, R.W., Austin, W.E.N., Ramsey, C.B., Grootes, P.M., Hughen, K.A., Kromer, B., Reimer, P.J., Adkins, J.F., Burke, A., Cook, M.S., Olsen, J., Skinner, L.C., 2020. Marine20 - the marine radiocarbon age calibration curve (0-55,000 cal BP). Radiocarbon. https://doi.org/10.1017/RDC.2020.68.

Hillenbrand, C.-D., Moreton, S.G., Caburlotto, A., Pudsey, C.J., Lucchi, R.G., Smellie, J.L., Benetti, S., Grobe, H., Hunt, J.B., Larter, R.D., 2008. Volcanic time-markers for Marine Isotopic Stages 6 and 5 in Southern Ocean sediments and Antarctic ice cores: implications for tephra correlations between palaeoclimatic records. Quat. Sci. Rev. 27, 518–540. https://doi.org/10.1016/j.quascirev.2007.11.009.

Hopfenblatt, J., Geyer, A., Aulinas, M., Álvarez-Valero, A.M., Sánchez, A.P., Giralt, S., Smellie, J.L., 2022. DecTephra: a new database of Deception Island's tephra record (Antarctica). J. Volcanol. Geoth. Res. 425, 107516 https://doi.org/10.1016/J.JVOLGEORES.2022.107516.

Hunt, J.B., Hill, P.G., 1993. Tephra geochemistry: a discussion of some persistent analytical problems. Holocene 3, 271–278. https://doi.org/10.1177/095968369300300310.

Iverson, N.A., 2017. Characterization and Correlation of Englacial Tephra from Blue Ice Areas and Ice Cores, Antarctica Nels Anton Iverson Dissertation Submitted as Partial Fulfillment of the Requirements for the Degree of Doctor of Philosophy in Earth and Environmental Sc.

Jochum, K.P., Stoll, B., Herwig, K., Willbold, M., Hofmiann, A.W., Amini, M., Aarburg, S., Abouchami, W., Hellebrand, E., Mocek, B., Raczek, I., Stracke, A., Alard, O., Bouman, C., Becker, S., Dücking, M., Brätz, H., Klemd, R., De Bruin, D., Canil, D., Cornell, D., De Hoog, C.J., Dalpé, C., Danyushevshy, L., Eisenhauer, A., Gao, Y., Snow, J.E., Groschopf, N., Günther, D., Latkoczy, C., Guillong, M., Hauri, E.H., Höfer, H.E., Lahaye, Y., Horz, K., Jacob, D.E., Kasemann, S.A., Kent, A.J.R., Ludwig, T., Zack, T., Mason, P.R.D., Meixner, A., Rosner, M., Misawa, K., Nash, B.P., Pfänder, J., Premo, W.R., Sun, W.D., Tiepolo, M., Vannucci, R., Vennemann, T., Wayne, D., Woodhead, J.D., 2006. MPI-DING reference glasses for in situ microanalysis: new reference values for element concentrations and isotope ratios. G-cubed 7, 1–44. https://doi.org/10.1029/2005GC001060.

Jolliffe, I.T., Cadima, J., 2016. Principal component analysis: a review and recent developments. Philos. Tran.s A. Math. Phys. Eng. Sci. 13 (374), 20150202 https://doi.org/10.1098/rsta.2015.0202, 2065.

Koffman, B.G., Dowd, E.G., Osterberg, E.C., Ferris, D.G., Hartman, L.H., Wheatley, S.D., Kurbatov, A.V., Wong, G.J., Markle, B.R., Dunbar, N.W., Kreutz, K.J., Yates, M., 2017. Rapid transport of ash and sulfate from the 2011 Puyehue-Cordón Caulle (Chile) eruption to West Antarctica. J. Geophys. Res. Atmos. 122, 8908–8920. https://doi.org/10.1002/2017JD026893.

LeBas, M.J.L., Maitre, R.W.L., Streckeisen, A., Zanettin, B., 1986. A chemical classification of volcanic rocks based on the total alkali-silica diagram. J. Petrol. 27, 745–750. https://doi.org/10.1093/petrology/27.3.745.

Lee, M.J., Kyle, P.R., Iverson, N.A., Lee, J.I., Han, Y., 2019. Rittmann volcano, Antarctica as the source of a widespread 1252 ± 2 CE tephra layer in Antarctica ice. Earth Planet Sci. Lett. 521, 169–176. https://doi.org/10.1016/j.epsl.2019.06.002.

McDonough, W.F., Sun, S. -s., 1995. The composition of the Earth. Chem. Geol. 122, 223–253. https://doi.org/10.1016/0009-2541(94)00140-4.

Mezgec, K., Stenni, B., Crosta, X., Masson-Delmotte, V., Baroni, C., Braida, M., Ciardini, V., Colizza, E., Melis, R., Salvatore, M.C., Severi, M., Scarchilli, C., Traversi, R., Udisti, R., Frezzotti, M., 2017. Holocene sea ice variability driven by wind and polynya efficiency in the Ross Sea. Nat. Commun. 8, 1334. https://doi.org/10.1038/s41467-017-01455-x.

Morelli, D., Colizza, E., Corradi, N., Finocchiaro, F., Giglio, F., Langone, L., Ridente, D., 2008. Morpho-stratigraphic features of the Edisto inlet, a high sedimentation rate site in the western Ross Sea (Antarctica). EGS-AGU-EUG Joint Assembly, Vienna, Austria, April 2008 Geophys. Res. Abstr. 10, 07252 (Poster).

Moreton, S.G., Smellie, J.L., 1998. Identification and correlation of distal tephra layers in deep-sea sediment cores, Scotia Sea, Antarctica. Ann. Glaciol. 27, 285–289. https://doi.org/10.3189/1998AoG27-1-285-289.

Narcisi, B., Petit, J.R., Delmonte, B., Basile-doelsch, I., Maggi, V., 2005. Characteristics and sources of tephra layers in the EPICA-Dome C ice record (East Antarctica): implications for past atmospheric circulation and ice core. stratigraphic correlations 239, 253–265. https://doi.org/10.1016/j.epsl.2005.09.005.

Narcisi, B., Petit, J.R., Chappellaz, J., 2010. A 70 ka record of explosive eruptions from the TALDICE ice core (Talos Dome, East Antarctic plateau). J. Quat. Sci. 25, 844–849. https://doi.org/10.1002/jqs.1427, 2010.

Narcisi, B., Petit, J.R., Delmonte, B., Scarchilli, C., Stenni, B., 2012. A 16,000-yr tephra framework for the Antarctic ice sheet: a contribution from the new Talos Dome core. Quat. Sci. Rev. 49, 52–63. https://doi.org/10.1016/j.quascirev.2012.06.011.

Narcisi, B., Petit, J.R., Langone, A., 2017. Last glacial tephra layers in the Talos Dome ice core (peripheral East Antarctic Plateau), with implications for chronostratigraphic correlations and regional volcanic history. Quat. Sci. Rev. 165, 111–126. https://doi.org/10.1016/j.quascirev.2017.04.025.

Narcisi, B., Petit, J.R., Delmonte, B., Batanova, V., Savarino, J., 2019. Multiple sources for tephra from AD 1259 volcanic signal in Antarctic ice cores. Quat. Sci. Rev. 210, 164–174. https://doi.org/10.1016/J.QUASCIREV.2019.03.005.

Obreht, I., Hambach, U., Veres, D., Zeeden, C., Bösken, J., Stevens, T., Marković, S.B., Klasen, N., Brill, D., Burow, C., Lehmkuhl, F., 2017. Shift of large-scale atmospheric systems over Europe during late MIS 3 and implications for Modern Human dispersal. Sci. Rep. 7, 5848. https://doi.org/10.1038/s41598-017-06285-x.

Oppedal, L.T., van der Bilt, W.G.M., Balascio, N.L., Bakke, J., 2018. Patagonian ash on sub-Antarctic South Georgia: expanding the tephrostratigraphy of southern South America into the Atlantic sector of the Southern Ocean. J. Quat. Sci. 33, 482–486. https://doi.org/10.1002/jqs.3035.

Pearce, N.J.G., Perkins, W.T., Westgate, J.A., Gorton, M.P., Jackson, S.E., Neal, C.R., Chenery, S.P., 1997. A compilation of new and published major and trace element data for NIST SRM 610 and NIST SRM 612 glass reference materials. Geostand. Newsl. 21, 115–144. https://doi.org/10.1111/j.1751-908X.1997.tb00538.x.

Petrelli, M., Laeger, K., Perugini, D., 2016a. High spatial resolution trace element determination of geological samples by laser ablation quadrupole plasma mass spectrometry: implications for glass analysis in volcanic products. Geosci. J. 20, 851–863. https://doi.org/10.1007/s12303-016-0007-z.

Petrelli, M., Morgavi, D., Vetere, F., Perugini, D., 2016b. Elemental imaging and petro-volcanological applications of an improved laser ablation inductively coupled quadrupole plasma mass spectrometry. Period. Mineral. 85, 25–39. https://doi.org/10.2451/2015PM0465.

Plunkett, G., Sigl, M., Pilcher, J.R., McConnell, J.R., Chellman, N., Steffensen, J.P., Büntgen, U., 2020. Smoking guns and volcanic ash: the importance of sparse tephras in Greenland ice cores. Polar Res. 39, 3511. https://doi.org/10.33265/polar.v39.3511.

Reimer, P.J., Bard, E., Bayliss, A., Beck, J.W., Blackwell, P.G., Ramsey, C.B., Buck, C.E., Cheng, H., Edwards, R.L., Friedrich, M., Grootes, P.M., Guilderson, T.P., Haflidason, H., Hajdas, I., Hatté, C., Heaton, T.J., Hoffmann, D.L., Hogg, A.G., Hughen, K.A., Kaiser, K.F., Kromer, B., Manning, S.W., Niu, M., Reimer, R.W., Richards, D.A., Scott, E.M., Southon, J.R., Staff, R.A., Turney, C.S.M., van der Plicht, J., 2013. IntCal13 and Marine13 radiocarbon age calibration curves 0–50,000 Years cal BP. Radiocarbon 55, 1869–1887. https://doi.org/10.2458/azu_js_rc.55.16947.

Tesi, T., Belt, S.T., Gariboldi, K., Muschitiello, F., Smik, L., Finocchiaro, F., Giglio, F., Colizza, E., Gazzurra, G., Giordano, P., Morigi, C., Capotondi, L., Nogarotto, A., Köseoğlu, D., Di Roberto, A., Gallerani, A., Langone, L., 2020. Resolving sea ice dynamics in the north-western Ross Sea during the last 2.6 ka: from seasonal to millennial timescales. Quat. Sci. Rev. 237, 106299 https://doi.org/10.1016/j.quascirev.2020.106299.

Wilch, T.I., McIntosh, W.C., Dunbar, N.W., 1999. Late quaternary volcanic activity in Marie Byrd land: potential 40 Ar/39 Ar-dated time horizons in West Antarctic ice and marine cores. Bull. Geol. Soc. Am. 111, 1563–1580. https://doi.org/10.1130/0016-7606(1999)111<1563:LQVAIM>2.3.CO, 2.